Influence of Thickness and Camber on the Aeroelastic Stability of Supersonic Throughflow Fans

John K. Ramsey*
NASA Lewis Research Center, Cleveland, Ohio 44135

An engineering approach was used to include the nonlinear effects of thickness and camber in an analysis of cascades in supersonic axial flow (supersonic leading-edge locus). A hybrid code using Lighthill's nonlinear piston theory and Lane's linear potential theory was developed to include these nonlinear effects. Lighthill's theory was used to calculate the unsteady pressures on the noninterference surface regions of the airfoils in cascade. Lane's theory was used to calculate the unsteady pressures on the remaining interference surface regions. Two airfoil profiles were investigated: a supersonic throughflow fan design and a NACA 66-206 airfoil with a sharp leading edge. Results show that compared with predictions of Lane's potential theory for flat plates, the inclusion of thickness (with or without camber) may increase or decrease the aeroelastic stability depending on the airfoil geometry and operating conditions. When thickness effects are included in the aeroelastic analysis, inclusion of camber will influence the predicted stability in proportion to the magnitude of the added camber. The critical interblade phase angle, depending on the airfoil profile and operating conditions, may also be influenced by thickness and camber.

Nomenclature

A = $2BY_1$, see Fig. 1
a_e = elastic axis position referenced from half chord, see Fig. 5
a_∞ = freestream speed of sound
B = $\sqrt{M^2-1}$
b = half chord
C = coefficients in power series describing airfoil surface slope
c = chord
$f(x)^{(\pm)}$ = function describing steady-state upper suction (+) and lower pressure (−) airfoil surfaces, positive away from airfoil on each side
g = circumferential gap between adjacent blades
h_{ar} = plunging amplitude in rth mode
h_s = plunging amplitude of the sth blade
$I_{\alpha s}$ = polar moment of inertia about elastic axis of sth blade
i = imaginary unit
J_0 = Bessel function of the first kind of order 0
k_b = reduced frequency, based on half chord, $= \omega b/U_\infty$
k_c = reduced frequency, based on chord, $= \omega c/U_\infty$
k_{hs} = bending stiffness of sth blade
$k_{\alpha s}$ = torsional stiffness of sth blade
L_s = aerodynamic lift of sth blade
l_{hhr}, $l_{h\alpha r}$ = nondimensional lift coefficients in rth mode due to plunging and pitching motions, respectively
$l_{\alpha hr}$, $l_{\alpha\alpha r}$ = nondimensional moment coefficients in rth mode due to plunging and pitching motions, respectively
M = relative Mach number
M_s = aerodynamic moment of sth blade
m_s = mass per unit span of sth blade
N = number of blades
$p'^{(\pm)}$ = unsteady pressure on the upper suction (+) and lower pressure (−) airfoil surfaces, respectively
p_∞ = freestream static pressure
R = specific gas constant
r = integer specifying mode
$r_{\alpha s}$ = nondimensional radius of gyration of sth blade
$S_{\alpha s}$ = mass moment about elastic axis ($m_s b x_{\alpha s}$) of sth blade
s = blade index
T_∞ = freestream static temperature
t = time
U_∞ = freestream air velocity relative to blade
U_r = reduced velocity, $= U_\infty/\omega b$
W = total normal velocity
w' = unsteady normal velocity (downwash)
x = streamwise coordinate
x_0 = streamwise coordinate of elastic axis referenced from the airfoil leading edge, $= b + a_e b$
$x_{\alpha s}$ = nondimensional static unbalance of sth blade
Y = transverse coordinate
α = complex amplitude of incidence, $= w'$
$\bar{\alpha}$ = steady-state angle of attack
α_{ar} = pitching amplitude in rth mode
α_s = pitching amplitude of sth blade
β_r = interblade phase angle of rth mode
γ = ratio of specific heats (assume = 1.4)
ϵ = maximum displacement in airfoil oscillation
ϵ_n = 1 if $n = 0$; 2 if $n \geq 1$
ζ = dummy variable of integration
ζ_{hs} = critical damping ratio for bending mode of sth blade
$\zeta_{\alpha s}$ = critical damping ratio for torsional mode of sth blade
$\theta^{(\pm)}$ = steady-state slope of airfoil surface with respect to the freestream (positive for compression waves, negative for expansion waves) on upper suction (+) and lower pressure (−) airfoil surfaces
κ = $k_c M/B^2$
μ = mass ratio, $= m_s/\pi\ \rho_\infty b^2$
ξ = stagger angle
ρ_∞ = freestream air density
σ = interblade phase angle
τ = thickness to chord ratio for biconvex airfoil
Ω = $\sigma + 2\kappa M x_1$ (x_1 shown in Fig. 1)

Received March 27, 1989; revision received Feb. 5, 1990.

*Research Engineer.

ω = circular frequency
ω_{hs} = bending frequency of sth blade
$\omega_{\alpha s}$ = torsional frequency of sth blade
1[ ] = symmetrical unit step function

Introduction

In recent years, there has been increased interest in providing efficient supersonic propulsion technology for supersonic transport applications. Needless to say, there are major challenges in this effort to provide new technology. One concept that shows considerable promise is the Supersonic Throughflow Fan (SSTF) Engine. A detailed description of this engine and its benefits as well as associated research is given in Refs. 1 and 2 and briefly described here. This engine concept, if successful, will realize a 12% improvement in installed specific fuel consumption and a 25% reduction in installed weight as compared to a nonafterburning turbofan. The SSTF, being a necessary component of the SSTF engine, will efficiently process the the intake airflow at supersonic throughflow velocities, thereby eliminating the need for a conventional supersonic inlet system. Thus, the inlet weight realized by using the SSTF will be about one-half that of conventional supersonic inlets. Other advantages include fewer fan stages required to achieve a given pressure ratio, less boundary-layer bleed drag, better inlet pressure recovery, and better matching of bypass ratio variations to flight Mach number.

Previous experimental research on the SSTF concept is extremely limited.[3-5] Therefore, to evaluate the concept and potential of the SSTF, there is currently a research effort to design, build, and test a SSTF.[6,7] During the original design of the rotor blades, aeroelastic stability became a concern. Consequently, a linear two-dimensional unsteady potential theory presented by Lane[8] was developed into a computer program[9] and incorporated into an existing aeroelastic code for use in the aeroelastic stability analysis of the SSTF.[10] The blades were shown to be unstable, and consequently, were redesigned. This analysis considered the cascade of blades to be flat plates. In an effort to improve our analysis capabilities, it was desired to incorporate the effects of thickness and camber into our aeroelastic model.

A limited amount of analytical research has been performed in the area of unsteady supersonic flow in cascades, with supersonic leading-edge locus (SLEL).[8-18] This previous analytical work has been limited to flat-plate airfoil geometries. Currently, there is an effort to couple supersonic versions of computational fluid dynamic (CFD) codes[19-21] with a structural dynamic code (time domain)[22] to computationally solve the problem at hand. However, this effort is in its early stages. It is doubtful that in the near future CFD-structural dynamic tools, when fully developed, will be used for initial aeroelastic calculations. To calculate the flutter point in torsion of the original SSTF with 58 blades, using the CFD[19]-structural dynamic approach, a large amount of CPU time would be required on the Cray XMP.[23] Therefore, it is envisioned that CFD-structural dynamic codes will be used to refine the flutter boundaries predicted by much more simple and efficient analytical codes. It has been wisely suggested[24] that the next major research effort to include the effects of thickness and camber into aeroelastic stability analysis would be to use a linearized class of analysis codes based on Refs. 25 and 26. Such an analysis would linearize the unsteady flow about a nonlinear steady flow. This could be done using the method of characteristics with Ref. 27 providing the basis for the nonlinear steady flow. The linearized Euler method presented in Ref. 28, which accounts for airfoil geometry, may also be extended to the case of supersonic axial flow. As such, these analyses would include thickness and camber effects for the entire airfoil.

Although these methods would be more computationally intensive than the linear codes, they would take much less CPU time than the CFD-structural dynamic approach. However, to the author's knowledge, this type of analysis has not yet been extended to the case of supersonic axial flow.

The dilemma, therefore, is that the coupled CFD-structural dynamic codes, which include nonlinear thickness and camber effects, are not yet fully realized and when developed will be computationally lengthy, whereas the linear analytical codes available, which take much less CPU time, do not include nonlinear thickness and camber effects. Also, extending the linearized class of analysis described earlier[25,26,28] to the case of supersonic axial flow would take more time than the urgency of the flutter analysis permitted. Therefore, as a first attempt at including thickness and camber effects in an aeroelastic stability analysis for cascades with SLEL, and also as a means of getting results at the present, Lighthill's nonlinear piston theory was utilized.[24] As a result, the existing unsteady aerodynamic code[9] was modified to include the nonlinear piston theory.

Nonlinear Piston Theory

More than one nonlinear unsteady aerodynamic theory for isolated airfoils exists. Three that are known to the author are Van Dyke's theory,[29] Lighthill's nonlinear piston theory,[30-33] and Landahl's theory.[34] The simplicity of Lighthill's nonlinear piston theory is evident from Refs. 30 and 31, where it is shown that the analytical expression for the unsteady pressure is a simple function of Mach number and slope of the airfoil surface. In Ref. 32, Fig. 8, Ashley compares an experimental flutter point for a wing with various theories: piston theory (zero thickness), piston theory (with thickness), and exact linearized theory (Garrick and Rubinow[35]). It was shown that the piston theory (with thickness) agrees most closely with the experimental flutter point for the Mach number slightly less than 2. Thus, because of its simplicity and accuracy with respect to flutter calculations, Lighthill's nonlinear piston theory was used to predict the unsteady pressure distribution in the noninterference surface regions of the airfoils.

A brief review of Lighthill's theory will be described here for the reader's convenience. The normal velocity at any point on the airfoil surface is given by

$$W = U_\infty \theta + w' \tag{1}$$

where θ is positive for compression waves and negative for expansion waves. Thus, for an airfoil in steady state with upper (+) and lower (−) surfaces given by $f(x)^{(\pm)}$ and un-

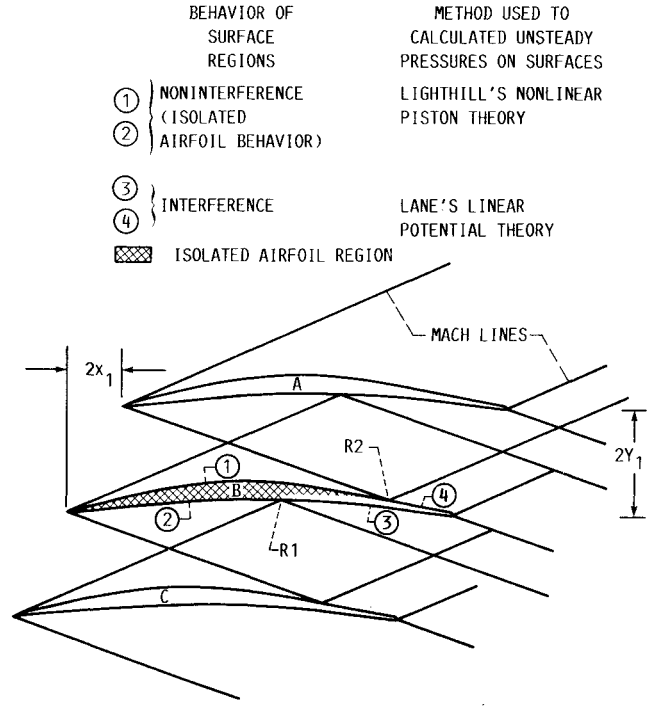

Fig. 1 Cascade in supersonic axial flow.

steady displacement $h = Y(x,t)$, the slope and unsteady downwash for the upper (suction) and lower (pressure) surfaces are

$$\theta^{(\pm)} = f_x(x)^{(\pm)} \mp \bar{\alpha} \tag{2}$$

$$w'^{(\pm)} = \mp\left(U_\infty \frac{\partial}{\partial x} + \frac{\partial}{\partial t}\right) Y(x,t) \tag{3}$$

$\bar{\alpha}$ is not utilized in the present work. As presented in Ref. 30, the pressure on the airfoil surface is given by

$$p = p_\infty \left(1 + \frac{\gamma - 1}{2}\frac{W}{a_\infty}\right)^{2\gamma/\gamma - 1} \tag{4}$$

By expanding Eq. (4) in a binomial series, substituting W in the expansion with Eq. (1), retaining terms linear in w', and making use of the following relations

$$p_\infty = \rho_\infty R T_\infty, \qquad a_\infty = \sqrt{\gamma R T_\infty}, \qquad U_\infty = M a_\infty$$

the unsteady pressure on the airfoil surface becomes[31]

$$p'^{(\pm)} = \mp \rho_\infty a_\infty \left(1 + \frac{\gamma + 1}{2} M\theta + \frac{\gamma + 1}{4} M^2\theta^2\right) w' \tag{5}$$

The well-known expression for downwash w' is given as

$$w' = U_\infty \left\{\alpha_s + ik_c\left[\frac{h_s}{c} + \alpha_s\left(\frac{x}{c} - \frac{x_0}{c}\right)\right]\right\} e^{i\omega t} \tag{6}$$

Substituting w' in Eq. (5) with Eq. (6), the equation for the unsteady pressure becomes

$$p'^{(\pm)} = \mp \rho_\infty U_\infty^2 \left(\frac{1}{M} + \frac{\gamma + 1}{2}\theta + \frac{\gamma + 1}{4} M\theta^2\right) \times \left\{\alpha_s + ik_c\left[\frac{h_s}{c} + \alpha_s\left(\frac{x}{c} - \frac{x_0}{c}\right)\right]\right\} e^{i\omega t} \tag{7}$$

This expression was used for calculating the unsteady pressures on the noninterference surface regions of the airfoils in cascade.

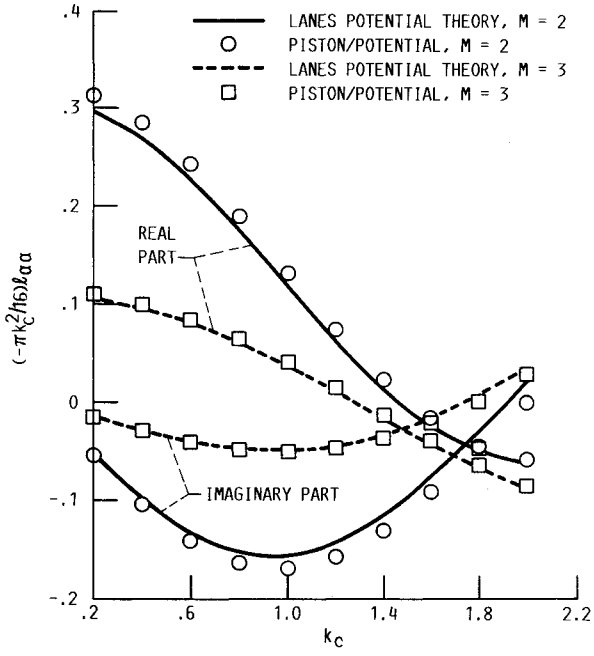

Fig. 2 Moment coefficients due to pitching motion about midchord for the SSTF (flat plate cascade) with interblade phase angle of 180 deg.

Table 1 Cascade parameters

Parameter	SSTF	NACA
N	58	10
μ	456.2	456.2
$r_{\alpha s}$	0.431	0.431
ξ, deg	28.0	28.0
g/c	0.311	0.311
$\omega_{hs}/\omega_{\alpha s}$	0.5668	0.5668
a_e	0	0
$x_{\alpha s}$	0	0

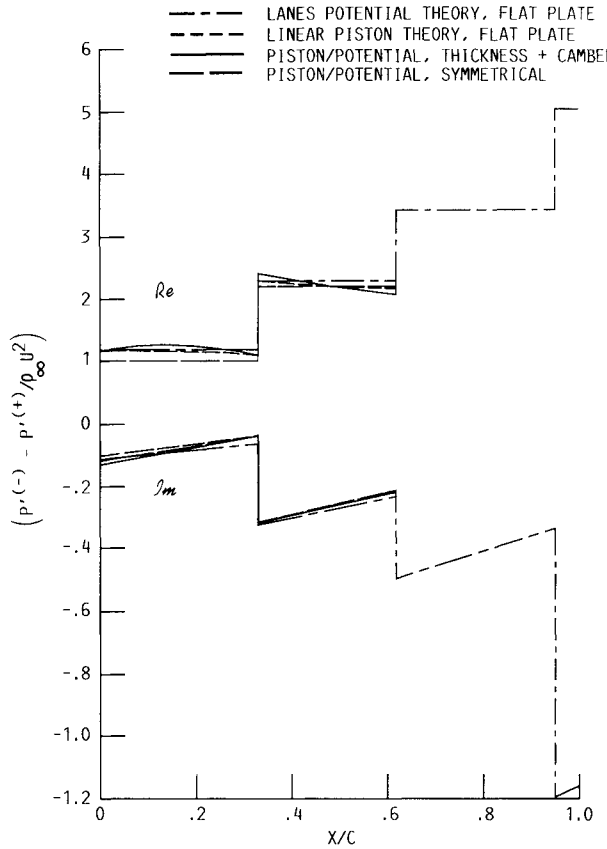

Fig. 3 Real and imaginary part of pressure difference for the SSTF at $M = 2$, $K_b = 0.1$, and interblade phase angle = 180 deg.

Approach

Shown in Fig. 1 is a schematic diagram of a cascade of airfoils in supersonic axial flow with SLEL. As shown, there are portions of each airfoil surface that are noninterference surfaces. As such, these surfaces behave as if the airfoil was isolated from its neighbors. In particular, the unsteady pressure distribution on surface regions 1 and 2 of airfoil B are not influenced by the presence of airfoils A and C. It is therefore true that the unsteady pressure on surface regions 1 and 2 are not influenced by interblade phase angle. The unsteady pressure on regions 1 and 2 of the airfoil can therefore be calculated using a nonlinear isolated airfoil theory that includes thickness and camber effects. The unsteady pressure on the remainder of the airfoil (surface regions 3 and 4) can be calculated using a linear flat-plate theory. The unsteady pressure distribution was generated by these two separate theories. In addition, the Mach lines are assumed to reflect off of the airfoils at the same chordwise locations and in the same manner that is predicted by Lane's theory[8] using flat plates. Up to Mach line reflection $R1$, as shown in Fig. 1, piston theory is used to calculate the unsteady pressure difference from the suction (upper) and pressure (lower) airfoil surfaces using Eq. (7). As shown in Fig. 1, for cascades with stagger, the isolated

airfoil surface region 1 on the upper surface will be a larger portion of the chord length as compared to the isolated surface region 2 on the lower surface. Because of this the unsteady pressure difference in the region between Mach line reflections, $R1$ and $R2$ must be calculated using both Lane's linear potential theory and Lighthill's nonlinear piston theory. Piston theory is used to calculate the upper airfoil surface contribution to the unsteady pressure difference in the region between Mach line reflections $R1$ and $R2$ using Eq. (7). Linear potential theory is used to calculate the lower airfoil surface contribution to the unsteady pressure difference in the region between Mach line reflections $R1$ and $R2$ using the following equation:

$$p'^{(-)} = -\rho_\infty U_\infty^2 \left(\frac{\partial}{\partial x} + ik_c\right) \int_0^x B^{-1}\alpha(\zeta) \times \Bigg[\exp\{-i[\kappa M(x-\zeta)+\Omega]\} \times 2\sum_{n=0}^{\infty} J_0\left\{\kappa\sqrt{(x+2x_1-\zeta)^2-(1+2n)^2A^2}\right\} \times 1[x+2x_1-\zeta-(1+2n)A] - \exp[-i\kappa M(x-\zeta)] \sum_{n=0}^{\infty} \epsilon_n J_0\left\{\kappa\sqrt{(x-\zeta)^2-4n^2A^2}\right\} \times 1[x-\zeta-2nA]\Bigg] d\zeta \quad (8)$$

Equation (8) describes the lower surface contribution to the unsteady pressure difference as predicted by Lane's linear potential theory. This equation was backed out of Lane's equations in Ref. 8. After Mach line reflection $R2$, the unsteady pressure difference from the upper and lower airfoil surfaces is calculated using the expanded form of Eq. (13) from Ref. 8 presented in Ref. 9 as Eq. (7).

Lane derived Eq. (13) in Ref. 8 for the unsteady pressure difference such that no information need be transferred across Mach lines or Mach line reflections. It is sufficient to specify the chordwise location x on the airfoil at which the unsteady pressure difference is desired in addition to the variables x_1, y_1, σ, k_c, M, and B, as illustrated in Eq. (8). Because of this, no interface was used across Mach lines or Mach line reflections between the nonlinear piston theory and the linear potential theory. The unsteady aerodynamic code was modified in such a way that the unsteady pressure after Mach line reflections $R1$ and $R2$, as predicted by Lane's potential theory, was not affected by the type of unsteady aerodynamic theory used to predict the unsteady pressure ahead of the Mach line reflections. Essentially, the unsteady pressure calculated using a combination of the nonlinear piston and linear potential theories is equivalent to calculating the unsteady pressure over the entire airfoil using Lane's linear potential theory, erasing the unsteady pressure up to Mach line reflections $R1$ and $R2$, and then replacing the unsteady pressures up to Mach line reflections $R1$ and $R2$ with that predicted by nonlinear piston theory. Therefore, this approach should be considered as an engineering approximation to the unsteady pressure distribution.[24]

Limitations of Approach

The assumptions Lighthill made in deriving his nonlinear theory may be found in Refs. 30 and 31. As a result of these assumptions, two limitations must be adhered to when using Lighthill's piston theory. The first limitation is that the airfoil total normal velocity must be less than the freestream speed of sound. This limiting condition is given as

$$M[\theta + (\epsilon/c)k_c] < 1$$

in Ref. 30 (Lighthill considers the theory to still have value as a rough approximation even when the left side is >1). Since ϵ is assumed to be extremely small for flutter analysis, the previous limitation is reduced to $M|\theta| < 1$, which agrees with Ref. 31.

There is also a limitation on the Mach number range in which Lighthill's nonlinear piston theory is applicable. Miles[31] states that Lighthill's piston theory can be used for flutter analysis at Mach numbers as low as 2. Morgan et al.[36] show that flutter calculations for a biconvex airfoil calculated by the theories of Van Dyke,[29] Landahl,[34] and Lighthill[30] show good agreement for $M > 2$–3. Ashley and Zartarian[32] showed that Lighthill's nonlinear piston theory exhibited good correlation with an experimental flutter point at a Mach number slightly less than 2. Zartarian et al.[33] recommend Lighthill's piston theory for trend analysis and preliminary design purposes even in parameter ranges where it lacks enough quantitative accuracy for precise calculations. Scruton et al.[37] showed that the aerodynamic stiffness and damping derivatives predicted by Lighthill's nonlinear piston theory are in reasonably good agreement with Van Dyke's theory[29] at $M = 2.43$. The damping derivative predicted by Lighthill's theory also showed good agreement with Van Dyke's theory at $M = 1.79$ for a single wedge airfoil pitching about midchord.[37] In light of these statements, a lower bound of $M = 2$ was set for this present work.

There are also certain limitations on the analysis due to the fact that the nonlinear thickness and camber effects are introduced into the analysis in the noninterference surface regions only. It should be mentioned that, for a given cascade geometry and low Mach number, the noninterference region of the airfoil is a small portion of the overall chord length. At some greater Mach number, depending on the cascade geometry, the entire airfoil is isolated (the noninterference surface region is the length of the entire chord). It would be expected that for low Mach numbers, the nonlinear portion of the analysis will have little influence on the overall stability calculations. As the Mach number increases, the nonlinear portion of the analysis has more influence.

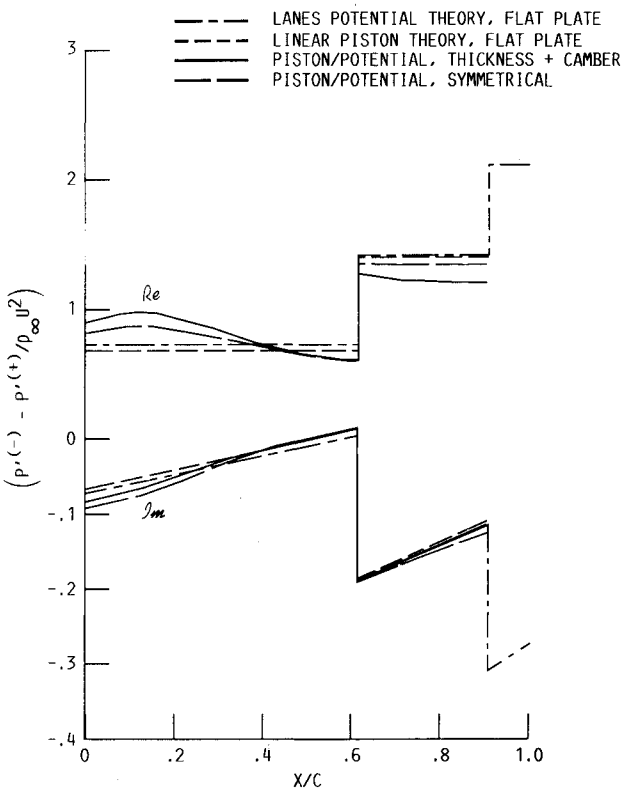

Fig. 4 Real and imaginary part of pressure difference for the SSTF at $M = 2.95$, $K_b = 0.1$, and interblade phase angle = 180 deg.

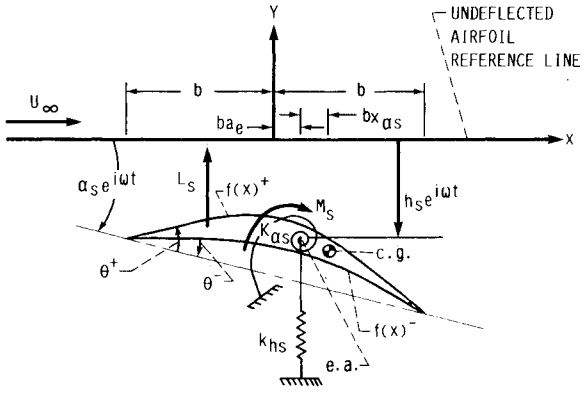

Fig. 5 Typical section.

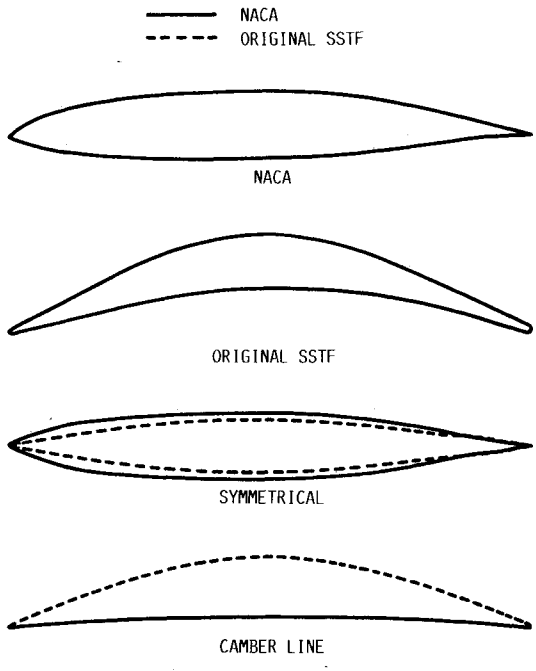

Fig. 6 Airfoil profiles and camber lines.

Code Verification

As stated previously, the unsteady aerodynamic code[9] was modified to include Eqs. (7) and (8). This modified unsteady aerodynamic code will be denoted as code 2. From here on, the unsteady aerodynamic code that exclusively consists of Lane's theory[9] is denoted as code 1.

Code 2 was verified in several ways. First, to verify the nonlinear portion of the code, the imaginary part of the moment coefficient due to pitching motion for a biconvex airfoil (with $k_c = 1$) as predicted by code 2 was compared with Lighthill's[30] aerodynamic damping derivatives at Mach 2 with $\tau = 0.05$ and 0.1 and at Mach number of 3 with $\tau = 0.0\bar{3}$ and 0.1. In all cases, the difference was less than 1.59%.

Second, to verify that the piston theory subroutine was interacting properly in the existing code,[9] the moment coefficient and the unsteady pressure distributions due to pitching motion for a cascade of flat plates predicted by code 2 was compared against code 1 by setting $\theta = 0$ in code 2. The cascade parameters used are shown in Table 1. Setting $\theta = 0$ in code 2 reduces Lighthill's nonlinear piston theory to linear piston theory. Linear piston theory was not expected to agree closely with linear potential theory in the Mach number range ($2 \leq M \leq 3$), which is used in this comparison. However, general trends should still be similar. As shown in Figs. 2–4, the general trends in the moment coefficient and unsteady pressures are similar, validating that the piston theory subroutine is interacting properly within the code.

Structural Model

The classical typical section, as shown in Fig. 5, was used to model the structure. Each airfoil is assumed to be a two-dimensional oscillator supported by bending and torsional springs. The airfoil is assumed to be rigid in the chordwise direction. Coupling between bending and torsional motion is modeled through the offset distance between the center of gravity and the "elastic axis."

Equations of Motion

The equations of motion used are those presented in Ref. 38 and are

$$\begin{bmatrix} m_s & S_{\alpha s} \\ S_{\alpha s} & I_{\alpha s} \end{bmatrix} \begin{Bmatrix} \frac{d^2}{dt^2}(h_s e^{i\omega t}) \\ \frac{d^2}{dt^2}(\alpha_s e^{i\omega t}) \end{Bmatrix} + \begin{bmatrix} (1+2i\zeta_{hs})m_s\omega_{hs}^2 & 0 \\ 0 & (1+2i\zeta_{\alpha s})I_{\alpha s}\omega_{\alpha s}^2 \end{bmatrix} \times \begin{bmatrix} h_s e^{i\omega t} \\ \alpha_s e^{i\omega t} \end{bmatrix} = \begin{bmatrix} -L_s \\ M_s \end{bmatrix} \tag{9}$$

L_s and M_s are the aerodynamic lift and moment, respectively, expressed in terms of nondimensional coefficients as

$$L_s = -\pi\rho_\infty b^3\omega^2 \sum_{r=0}^{N-1} \left[l_{hhr}\frac{h_{ar}}{b} + l_{h\alpha r}\alpha_{ar} \right] \exp\,[i(\omega t + \beta_r s)] \tag{10}$$

$$M_s = \pi\rho_\infty b^4\omega^2 \sum_{r=0}^{N-1} \left[l_{\alpha hr}\frac{h_{ar}}{b} + l_{\alpha\alpha r}\alpha_{ar} \right] \exp\,[i(\omega t + \beta_r s)] \tag{11}$$

where the coefficients l_{hhr}, $l_{h\alpha r}$, $l_{\alpha hr}$, and $l_{\alpha\alpha r}$ are calculated by Lighthill's nonlinear piston theory and Lane's linear potential theory for given values of M, k_b, c/g, ξ, β_r, and a_e. For the sake of completeness, Eqs. (10) and (11) allow for structurally mistuned blades in cascade even though a mistuned cascade was not studied in this work. The aeroelastic stability of the system is determined by solving a complex eigenvalue problem, resulting from an equation [Eq. (9)] written for each blade. An existing code[39] that solves this complex eigenvalue problem was used in the present research. For additional details see Ref. 38.

Blade Parameters

Table 1 lists the various cascade parameters that were used for the aeroelastic analysis. These values are for the 73.3% span location of the original SSTF design. In order to study the

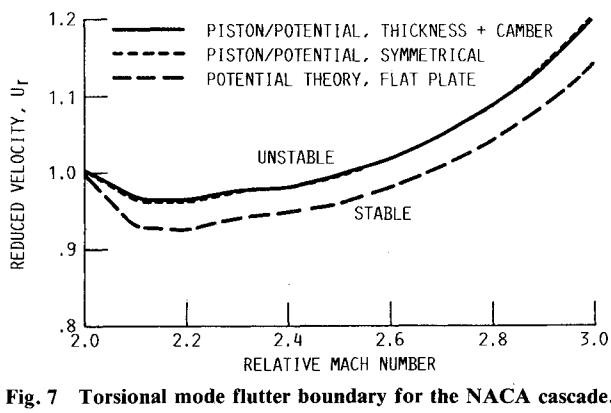

Fig. 7 Torsional mode flutter boundary for the NACA cascade.

Table 2 Series representation of NACA profiles

Coefficient[a]	Thickness and camber θ^+	Thickness and camber θ^-	Symmetrical $\theta^+(=\theta^-)$
C_1	0.27124	0.15037	0.210805
C_2	−1.86248	−1.32054	−1.591510
C_3	5.59980	4.66200	5.130900
C_4	−7.82200	−7.11520	−7.468600
C_5	3.72870	3.65935	3.694025

[a] $\theta = \sum_{\substack{i=1 \\ 0 \le x \le 1}}^{5} C_i x^{i-1}$

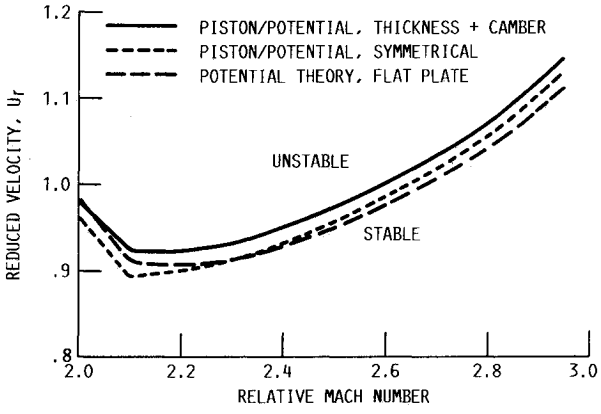

Fig. 8 Torsional mode flutter boundary for the SSTF.

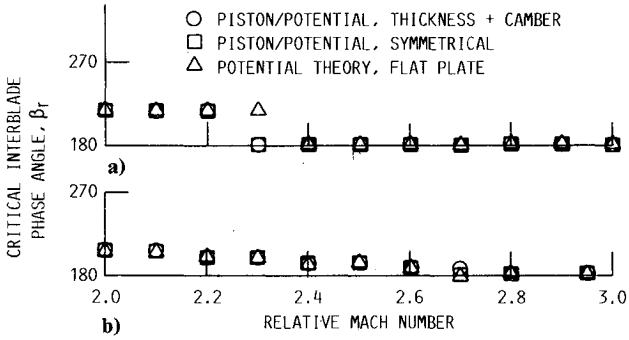

Fig. 9 Critical interblade phase angle as a function of Mach number for torsional mode flutter: a) NACA cascade; and b) SSTF.

effects of thickness and camber on the aeroelastic stability of an SSTF, some airfoil geometry having camber and thickness distributions must be chosen. The geometries used in the aeroelastic stability analysis were variations of a NACA 66-206 airfoil,[40] a flat plate, and variations of the original SSTF airfoil. These airfoil profiles and a comparison of the original SSTF and NACA airfoil camber lines are shown in Fig. 6. The NACA 66-206 as well as the original SSTF airfoil sections have surface slopes within the necessary criteria ($M|\theta| < 1$) previously mentioned. The NACA profile is assumed to have a sharp leading edge and not that as given in Ref. 40. The cascade parameters were held constant for all the airfoil profiles.

As already stated, the slopes of the suction and pressure airfoil surfaces are needed to compute the unsteady pressure on the noninterference surface regions. A 5 degree power series was fit to the coordinates of the suction and pressure surfaces of the NACA 66-206 as well as to the original SSTF airfoil. The resulting equations $f(x)^{(\pm)}$ were differentiated to give the slopes $[f_x(x)^{(\pm)} = \theta]$ of the suction and pressure surfaces as a function of chord location. The power series coefficients for the slopes of the NACA 66-206 profile with and without camber are shown in Table 2. These equations for the slopes were input to the aeroelastic code for use by the piston theory subroutine.

Results

The cascade consisting of the original 58 supersonic throughflow airfoils will be designated from here on as SSTF. The original SSTF airfoil profile is shown in Fig. 6. The cascade consisting of the 10 NACA 66-206 airfoils will be designated from here on as the NACA cascade. Its airfoil is also shown in Fig. 6. Only 10 blades were chosen for the NACA cascade to reduce computational effort.

As stated previously, the nonlinear portion of the code has more influence on the analysis as the Mach number increases. This is due to the fact that the noninterference surface regions of the airfoils, as shown in Fig. 1, increases with increasing Mach number. At a Mach number of 2, the noninterference surface region is approximately 60 and 30% of the suction and pressure surfaces, respectively. At a Mach number of 3, the noninterference surface region will be approximately 90 and 60% of the suction and pressure surfaces, respectively. Therefore, it can be concluded that, for this study, the nonlinear portion of the code will have a significant influence on the aeroelastic analysis. Indeed, at Mach 3, almost the entire unsteady pressure on the suction surface will be calculated by nonlinear piston theory.

Shown in Figs. 3 and 4 are the unsteady pressure distributions for torsional motion about midchord of the SSTF at $M = 2$ and $M = 2.95$ for $k_b = 0.1$ and interblade phase angle of 180 deg. Up to the first Mach line reflection, both upper and lower unsteady surface pressures are calculated using Lighthill's nonlinear piston theory. In the region between the first and second Mach line reflections $R1$ and $R2$, the unsteady pressure on the suction and pressure surfaces are calculated by nonlinear piston theory and potential theory, respectively. These plots are discussed in the following sections.

The flutter boundaries for torsional instability of the NACA cascade are shown in Fig. 7. The flutter boundaries for torsional instability of the original SSTF are shown in Fig. 8. Plots of critical interblade phase angle vs relative Mach number for the NACA cascade and SSTF are presented in Figs. 9a and 9b, respectively. These plots are discussed in the following sections.

Thickness Effect

It is shown in Fig. 6 that the thickness distribution for the NACA airfoil is larger than that for the original SSTF airfoil. Upon integration of the unsteady pressure distribution in Figs. 3 and 4, for the SSTF oscillating 180 deg out of phase at $k_b = 0.1$, it was found that thickness decreased the negative value (although still negative) of the real part of the moment coefficient $l_{\alpha\alpha}$ as compared to that predicted by Lane's theory for a flat-plate profile at Mach numbers of 2 and 2.95. Thickness increased the positive value of the imaginary part of $l_{\alpha\alpha}$ at Mach 2 and decreased its positive value (although still positive) at Mach 2.95 as compared to Lane's linear potential theory for a flat-plate profile.

As shown in Fig. 7, the inclusion of thickness (symmetrical profile) in the aeroelastic stability analysis increased the stability for the NACA cascade when compared to the analysis using Lane's potential theory for flat plates. The thickness distribution had more influence on the aeroelastic stability than did the camber when compared to the flat-plate analysis. As shown in Fig. 8, thickness (symmetrical profile) decreased the stability of the SSTF for $2 \le M \le 2.3$ and increased the stability at Mach numbers above 2.3 as compared to an analysis using Lane's theory for flat plates.

Camber Effects

As shown in Fig. 6, the camber of the original SSTF airfoil is much greater than that of the NACA airfoil. Upon integration of the unsteady pressure distribution in Figs. 3 and 4, for the SSTF cascade oscillating 180 deg out of phase at $k_b = 0.1$, it was found that adding camber to the thickness (symmetric)

distribution of the SSTF further decreased the negative value (although still negative) of the real part of the moment coefficient $l_{\alpha\alpha}$ as compared to the symmetric profile at $M=2$ and 2.95. At $M=2$, the addition of camber to the symmetric profile of the SSTF decreased the positive value (although still positive) of the imaginary part of $l_{\alpha\alpha}$ as compared to the symmetric profile, but was still larger than predicted by Lane's theory. At $M=2.95$, the addition of camber to the symmetric SSTF profile further decreased the positive value (although still positive) of the imaginary part of $l_{\alpha\alpha}$.

From Fig. 7, it is shown that the inclusion or exclusion of camber in the aeroelastic stability analysis of the NACA cascade, when thickness is included, has little effect on stability. This is not surprising since the camber of the NACA profile is small. However, as shown in Fig. 8, the inclusion or exclusion of camber in the aeroelastic stability analysis for the SSTF, when thickness is included, has a larger effect on stability as compared with the NACA cascade. This also is not surprising since the SSTF airfoil has more camber than the NACA airfoil. Including camber with thickness increased the predicted stability for the SSTF for Mach numbers slightly above 2.0 with respect to the analysis using Lane's theory for flat plates. The inclusion of camber with thickness also increased the stability of the SSTF when compared with the analysis with thickness only.

Interblade Phase Angle

As shown in Fig. 9a, the aeroelastic analysis of the NACA cascade including thickness with and without camber predicted a critical interblade phase angle of 216 deg from $M=2$–2.2. From $M=2.3$–3.0, the predicted critical interblade phase angle was 180 deg. The flat-plate analysis using Lane's theory predicted the same results except at $M=2.3$. Here, the aeroelastic analysis using the flat plate predicted a critical interblade phase angle of 216 deg as opposed to the aeroelastic analysis including thickness with or without camber, which predicted a critical interblade phase angle of 180 deg.

As shown in Fig. 9b, the aeroelastic analysis including thickness with or without camber predicted that the critical interblade phase angle of the SSTF decreases from 204.8 deg at $M=2$ to 180 deg at $M=2.95$. This is similar to the trend presented in Ref. 10. The aeroelastic analysis using flat plates predicted the same trend, except at $M=2.7$. Here, the aeroelastic analysis with thickness and camber resulted in a critical interblade phase angle of 186.2 deg as opposed to 180 deg from the analysis using flat plates and thickness only (symmetrical).

Conclusions

As a means of determining the influence of thickness and camber on the aeroelastic stability of supersonic throughflow fans, Lighthill's nonlinear piston theory, which includes thickness and camber effects, and Lane's linear potential theory have been developed into a hybrid unsteady aerodynamic code. This hybrid code, coupled with an existing aeroelastic code has been applied to a cascade of NACA 66-206 airfoils (NACA cascade) and a cascade consisting of the original supersonic throughflow fan airfoils (SSTF) in supersonic axial flow with supersonic leading-edge locus. Through this engineering approach, the effects of thickness and camber on the aeroelastic stability of supersonic throughflow fans have been investigated.

The major conclusions from this investigation are the following:

1) Depending on airfoil geometry and operating conditions, the inclusion of thickness with or without camber may either increase or decrease the predicted aeroelastic stability when compared to an analysis using Lane's potential theory for flat plates.

2) When thickness effects are included in the aeroelastic analysis, inclusion of camber will influence the predicted stability in proportion to the magnitude of the added camber.

3) The critical interblade phase angle, depending on the airfoil profile and operating conditions, may be influenced by thickness and camber.

4) Lane's linear potential theory for flat plates provided a conservative flutter boundary for both the NACA and SSTF cascades above $M=2$ and 2.3, respectively.

Acknowledgments

The author wishes to express his gratitude to John Adamczyk of NASA Lewis Research Center and M. F. Platzer of the Naval Postgraduate School, Monterey, California, whose ideas of using piston theory have made this paper possible. The author also wishes to express thanks to Robert E. Kielb of NASA Lewis Research Center for his valuable consultation and Michael A. Ernst of NASA Lewis Research Center for his valuable discussions.

References

[1]Franciscus, L., "The Supersonic Throughflow Turbofan for High Mach Propulsion," NASA TM-100114, July 1987.

[2]Ziemianski, J. A., Blaha, B. J., Batterton, P. G., Strack, W. C., Ball, C. L., Coltrin, R. E., and Northam, G. B., "High Speed Propulsion Technology," NASA CP-10003, 1987.

[3]Klapproth, J. F., "A Review of Supersonic Compressor Development," *Journal of Engineering for Power*, Vol. 83, No. 3, July 1961, pp. 258–268.

[4]Savage, M., Boxer, E., and Erwin, J. R., "Resume of Compressor Research at the NACA Langley Laboratory," *Journal of Engineering for Power*, Vol. 83, No. 3, July 1961, pp. 269–285.

[5]Breugelmans, F. A. E., "The Supersonic Axial Component in a Compressor," American Society of Mechanical Engineers, Paper 75-GT-26, March 1975.

[6]Schmidt, J. F., Moore, R. D., Wood, J. R., and Steinke, R. J., "Supersonic Through-Flow Fan Design," AIAA Paper 87-1746, July 1987.

[7]Wood, J. R., Schmidt, J. F., Steinke, R. J., Chima, R. V., Kunik, W. G., "Application of Advanced Computational Codes in the Design of an Experiment for a Supersonic Throughflow Fan Rotor," Gas Turbine Conference and Exhibition, Anaheim, CA, May 31–June 4, American Society of Mechanical Engineers, 87-GT-160, 1987.

[8]Lane, F., "Supersonic Flow Past an Oscillating Cascade with Supersonic Leading-Edge Locus," *Journal of Aeronautical Sciences*, Vol. 24, No. 1, 1957, pp. 65–66.

[9]Ramsey, J. K., and Kielb, R. E., "A Computer Program for Calculating Unsteady Aerodynamic Coefficients for Cascades in Supersonic Axial Flow," NASA TM-100204, corrected version, Dec. 1987.

[10]Kielb, R. E., and Ramsey J. K., "Flutter of a Fan Blade in Supersonic Axial Flow," *Journal of Turbomachinery*, Vol. 3, No. 4, 1989, pp. 462–667.

[11]Miles, J. W., "The Compressible Flow Past an Oscillating Airfoil in a Wind Tunnel," *Journal of Aeronautical Sciences*, Vol. 23, No. 7, 1956, pp. 671–678.

[12]Drake, D. G., "The Oscillating Two-Dimensional Aerofoil Between Porous Walls," *The Aeronautical Quarterly*, Vol. 8, No. 3, 1957, pp. 226–239.

[13]Gorelov, D. N., "Lattice of Plates in an Unsteady Supersonic Flow," *Fluid Dynamics*, Vol. 1, No. 4, 1966, pp. 34–39.

[14]Platzer, M. F., and Chalkley, H. G., "Theoretical Investigations of Supersonic Cascade Flutter and Related Interference Problems," AIAA Paper 72-377, April 1972.

[15]Chalkley, H. G., "A Study of Supersonic Flutter," Aeronautical Engineers Thesis, Naval Postgraduate School, Monterey, CA, June 1972.

[16] Nagashima, T., and Whitehead, D. S., "Linearized Supersonic Unsteady Flow in Cascades," Aeronautical Research Council, London, England, R&M-3811, Feb. 1977.

[17]Nishiyama, T., and Kikuchi, M., "Theoretical Analysis for Unsteady Characteristics of Oscillating Cascade Aerofoils in Supersonic Flows," *The Technology Reports of the Tohoku University*, Vol. 38, No. 2, 1973, pp. 565–597.

[18]Caruthers, J. E., "Theoretical Analysis of Unsteady Supersonic Flow Around Harmonically Oscillating Turbofan Cascades," Ph.D. Dissertation, Georgia Institute of Technology, Atlanta, GA, Sept. 1976.

[19]Huff, D. L., "Numerical Analysis of Supersonic Flow Through Oscillating Cascade Sections by Using a Deforming Grid," AIAA Paper 89-2805, July 1989.

[20]Whitfield, D. L., Swafford, T. W., Mulac, R. A., Belk, D. M., and Janus, J. M., "Three-Dimensional Unsteady Euler Solutions for Propfans and Counter-Rotating Propfans in Transonic Flow," AIAA Paper 87-1197, June 1987.

[21]Kao, Y. F., "Two Dimensional Unsteady Analysis for Transonic and Supersonic Cascade Flows," Ph.D. Dissertation, Purdue University, West Lafayette, IN, May 1989.

[22]Reddy, T. S. R., Srivastava, R., and Kaza, K. R. V., "The Effects of Rotational Flow, Viscosity, Thickness, and Shape on Transonic Flutter Dip Phenomena," AIAA Paper 88-2348, April 1988.

[23]Huff, D., Hoyniak, D., and Reddy, T.S., private communication, 1989.

[24]Adamczyk, J., and Platzer, M. F., private communication, 1989.

[25]Vogeler, F.-K., "Cascades with Harmonically Oscillating Blades in Supersonic Flow," NASA TT-20323, Aug. 1988.

[26]Verdon, J. M., "Linearized Unsteady Aerodynamic Theory," *AGARD Manual on Aeroelasticity in Axial-Flow Turbomachines: Vol. 1, Unsteady Turbomachinery Aerodynamics,* pp. 2-1-2-31.

[27]York, R. E., and Delaney, R. A., "A Research Note on the Flow Structure of Supersonic Compressor Cascade," Detroit Diesel Allison, Indianapolis, IN, RN 72-54, July 1972.

[28]Hall, K. C., and Crawley, E. F., "Calculation of Unsteady Flows in Turbomachinery Using the Linearized Euler Equations," *AIAA Journal*, Vol. 27, No. 6, 1989, pp. 777-787.

[29]Van Dyke, M., "Supersonic Flow Past Oscillating Airfoils Including Nonlinear Thickness Effects," NACA TN-2982, July 1953.

[30]Lighthill, M. J., "Oscillating Airfoils at High Mach Number," *Journal of the Aeronautical Sciences*, Vol. 20, June 1953.

[31]Miles, J. W., "Unsteady Flow at Hypersonic Speeds," *Proceedings of the Eleventh Symposium of the Colston Research Society*, edited by A. R. Collar and J. Tinkler, Academic Press, Orlando, FL, 1959, pp. 185-197.

[32]Ashley, H., and Zartarian, G., "Piston Theory—A New Aerodynamic Tool for Aeroelastician," *Journal of the Aeronautical Sciences*, Vol. 23, No. 12, Dec. 1956.

[33]Zartarian, G., Heller, A., and Ashley, H., "Application of Piston Theory to Certain Elementary Aeroelastic Problems," *Proceedings of the Fourth Midwestern Conference on Fluid Mechanics,* Purdue University, Lafayette, IN, Sept. 1955.

[34]Landahl, M., "Unsteady Flow Around Thin Wings at High Mach Numbers," *Journal of the Aeronautical Sciences*, Vol. 24, No. 1, Jan. 1957, pp. 33-38.

[35]Garrick, I. E., and Rubinow, S. I., "Flutter and Oscillating Air Force Calculations for an Airfoil in a Two-Dimensional Supersonic Flow," NACA TR-846, May 1946.

[36]Morgan, H., Runyan, H., and Huckel, V., "Theoretical Considerations of Flutter at High Mach Numbers," *Journal of the Aeronautical Sciences*, Vol. 25, June 1958, pp. 371-381.

[37]Scruton, C., Woodgate, L., Lapworth, K. C., and Maybrey, J., "Measurement of Pitching-Moment Derivatives for Aerofoils Oscillating in Two-Dimensional Supersonic Flow," Aeronautical Research Council, London, England, R&M 3234, Jan. 1959.

[38]Kaza, K. R. V., and Kielb, R. E., "Effects of Mistuning on Bending Torsion Flutter and Response of a Cascade in Incompressible Flow," *AIAA Journal*, Vol. 20, No. 8, 1982, pp. 1120-1127.

[39]"Miser2," COSMIC, University of Georgia, Athens, GA.

[40]Abbott, I. H., and Von Doenhoff, A. E., *Theory of Wing Sections*, Dover, New York, 1959, p. 441.